



Head-to-head comparison of [⁶⁸Ga]Ga-DOTA.SA.FAPi with [¹⁸F]F-FDG PET/CT in radioiodine-resistant follicular-cell derived thyroid cancers

Sanjana Ballal¹ · Madhav P. Yadav¹ · Frank Roesch² · Swayamjeet Satapathy¹ · Euy Sung Moon² · Marcel Martin² · Nicky Wakade¹ · Parvind Sheokand¹ · Madhavi Tripathi¹ · Kunal R. Chandekar¹ · Shipra Agarwal³ · Ranjit Kumar Sahoo⁴ · Sameer Rastogi⁴ · Chandrasekhar Bal¹

Received: 18 April 2023 / Accepted: 16 August 2023 / Published online: 29 August 2023
© The Author(s), under exclusive licence to Springer-Verlag GmbH Germany, part of Springer Nature 2023

Abstract

Purpose In the context of radioiodine-resistant follicular-cell derived thyroid cancers (RAI-R-FCTC), [¹⁸F]F-FDG PET/CT serves as a widely used and valuable diagnostic imaging method. However, there is growing interest in utilizing molecular imaging probes that target cancer-associated fibroblasts (CAFs) as an alternative approach. This study sought to compare the diagnostic capabilities of [⁶⁸Ga]Ga-DOTA.SA.FAPi and [¹⁸F]F-FDG PET/CT in patients with RAI-R-FCTC.

Methods In this retrospective study, a total of 117 patients with RAI-R-FCTC were included. The study population consisted of 68 females and 49 males, with a mean age of 53.2 ± 11.7 years. The aim of the study was to perform a comprehensive qualitative and quantitative assessment of [⁶⁸Ga]Ga-DOTA.SA.FAPi and [¹⁸F]F-FDG PET/CT scans in RAI-R-FCTC patients. The qualitative assessment involved comparing patient-based and lesion-based visual interpretations of both scans, while the quantitative assessment included analyzing standardized uptake values corrected for lean body mass (SUL_{peak} and SUL_{avg}). The findings obtained from the scans were validated by correlating them with morphological findings from diagnostic computed tomography and/or histopathological examination.

Results Among the 117 RAI-R-FCTC patients, 60 had unilateral local disease, and 9 had bilateral lesions with complete concordance in the detection rate on both PET scans. [⁶⁸Ga]Ga-DOTA.SA.FAPi had a higher detection rate for lymph nodes (95.4% vs 86.6%, *p*<0.0001), liver metastases (100% vs. 81.3%, *p*<0.0001), and brain metastases (100% vs. 39%, *p*<0.0001) compared to [¹⁸F]F-FDG. The detection rates for pleural and bone metastases were similar between the two radiotracers. For lung metastases, [⁶⁸Ga]Ga-DOTA.SA.FAPi showed a detection rate of 81.7%, whereas [¹⁸F]F-FDG had a detection rate of 64.6%. Remarkably, [⁶⁸Ga]Ga-DOTA.SA.FAPi was able to detect a bowel metastasis that was missed on [¹⁸F]F-FDG scan. The median standardized uptake values (SUL) were generally comparable between the two radiotracers, except for brain metastases (SUL_{peak} [⁶⁸Ga]Ga-DOTA.SA.FAPi vs. [¹⁸F]F-FDG: 13.9 vs. 6.7, *p*=0.0001) and muscle metastases (SUL_{peak} [⁶⁸Ga]Ga-DOTA.SA.FAPi vs. [¹⁸F]F-FDG: 9.56 vs. 5.62, *p*=0.0085), where [⁶⁸Ga]Ga-DOTA.SA.FAPi exhibited higher uptake.

Conclusion The study results demonstrate the superior performance of [⁶⁸Ga]Ga-DOTA.SA.FAPi compared to [¹⁸F]F-FDG PET/CT in detecting lymph nodal, liver, bowel, and brain metastases in patients with RAI-R-FCTC. These findings highlight the potential of [⁶⁸Ga]Ga-DOTA.SA.FAPi as a theranostic tool that can complement the benefits of [¹⁸F]F-FDG PET/CT in the imaging of RAI-R-FCTC.

Keywords [⁶⁸Ga]Ga-DOTA.SA.FAPi · [¹⁸F]F-FDG · Radioiodine-resistant follicular-cell derived thyroid cancer

Sanjana Ballal and Madhav P. Yadav contributed equally in the making of this manuscript.

A section of this project was released as a pre-print on Research Square. Sanjana Ballal, Madhav Yadav, Nicky Wakade et al. Head-to-head comparison of [⁶⁸Ga]Ga-DOTA.SA.FAPi with [¹⁸F]F-FDG PET/CT in radioiodine-resistant follicular-cell derived thyroid cancers, 06 February 2023, PREPRINT (version 1) available at Research Square [<https://doi.org/10.21203/rs.3.rs-2382675/v1>].

Extended author information available on the last page of the article

Introduction

Thyroid cancer is the most common endocrine malignancy with a 3:1 female-to-male ratio [1]. Among cancers originating from the thyroid's follicular cells, the majority (80–85%) are classified as papillary thyroid cancer, followed by follicular thyroid cancer (10–15%). Less common types include poorly differentiated thyroid cancer (<2%)

and undifferentiated (anaplastic) thyroid cancer (<2%) [2]. Surgical management followed by radioiodine (RAI) therapy has remained the mainstay treatment option in treating differentiated thyroid cancer (DTC) patients. DTC is capable of metabolizing radioiodine due to the presence of the sodium iodide symporter mechanism (NIS). This mechanism enables the uptake and utilization of radioiodine for treatment. Conversely, dedifferentiated and other types of thyroid cancers lack NIS expression, rendering them unable to metabolize radioiodine. These types of thyroid cancers are often referred to as radioiodine refractory or RAI negative.

Approximately 5 to 15% of locoregional DTC and 40–50% of metastatic DTCs are refractory to RAI [1, 3, 4]. Various mechanisms contribute to the inability of thyroid cancer (TC) to concentrate radioiodine. One such mechanism occurs in advanced-stage thyroid cancer, where tumor differentiation is higher, resulting in the loss of sodium iodide symporter (NIS) expression due to gene silencing within the NIS pathway. However, these malignant cells continue to metabolize glucose, as indicated by the expression of glucose transporter receptor type 1 (GLUT-1). Consequently, these cells uptake [¹⁸F]F-FDG, a glucose analog, which can be detected using positron emission tomography (PET) imaging [5]. This “flip-flop” phenomenon, characterized by high glucose uptake and low to no iodine uptake, is observed in dedifferentiated thyroid cancer and other aggressive variants such as poorly differentiated, Hürthle cell, and anaplastic thyroid cancer [6–8]. Currently, [¹⁸F]F-FDG PET/CT is the standard and valuable diagnostic imaging modality for radioiodine-negative thyroid cancer. It exhibits a sensitivity of 84% and a specificity of 78% in detecting RAI refractory disease [9]. However, it should be noted that false-positive findings occur in approximately 39% of patients, which is a limitation of [¹⁸F]F-FDG PET/CT [10].

In addition to genetic alterations, emerging evidence suggests that the development, growth, and advancement of thyroid cancer are significantly influenced by the cellular pathways involving the interaction between tumor cells and their surrounding tumor microenvironment (TME) [11]. Within the TME, cancer-associated fibroblasts (CAFs) play a crucial role and are considered key components. Cancer-associated fibroblasts (CAFs) are the key elements of TME and play a critical role in the progression of human cancers. In comparison to normal thyroid tissue, thyroid carcinomas exhibit an abnormal increase in CAFs.

Research investigating the expression of cancer-associated fibroblasts (CAFs) in human thyroid cancer tissue has revealed a strong association between the expression of CAF-related proteins and clinicopathological features. In a study by Cho et al. [12], the presence of CAFs was identified

as a significant predictive marker for lymph node metastases in thyroid cancer. Another study conducted by Sun et al. [13] found that thyroid cancer cases with the BRAFV600E mutation exhibited high expression of certain CAF-related proteins, including fibroblast activation protein- α (FAP- α). Sun et al. [13] also reported that stromal positivity for PDGFR- β was linked to shorter overall survival in papillary thyroid carcinoma (PTC).

The targeting of cancer-associated fibroblasts (CAFs) for imaging or treatment purposes involves interfering with CAF activation or inhibiting their functions. A promising approach in this regard is the use of FAP inhibitors (FAPI), which are small molecule radioligands that can be used for positron emission tomography (PET) imaging as well as radioligand therapy in various cancers. Molecular imaging probes specifically targeting CAFs have gained significant attention as a potential alternative to [¹⁸F]F-FDG PET/CT in oncology imaging. Notably, Veken et al. have developed FAP inhibitor structures based on the UAMC 1110 motif, which exhibits high selectivity for FAP and low affinity for related protease family members [14]. In recent years, several radiopharmaceuticals based on these FAP inhibitors have been developed by different research centers, including [⁶⁸Ga]Ga-labeled FAPI-02 [15], [⁶⁸Ga]Ga-labeled FAPI-04 [16], [⁶⁸Ga]Ga-labeled FAPI-46 [17], DOTA.SA.FAPi [18], and DOTAGA.(SA.FAPi)₂ [19], and have gained momentum for imaging various cancers. Studies have reported varying uptake patterns of these FAPi radiopharmaceuticals in thyroid cancers, with some authors observing high uptake profiles [18] while others, such as Giesel et al. [15] and Kratochwil et al. [16], reporting minimal uptake.

Due to the limited treatment options available for dedifferentiated aggressive thyroid cancers, there is a need to develop theranostic probes that can provide both imaging and treatment capabilities for thyroid cancer [20]. With only a few studies in the literature discussing the use of [⁶⁸Ga]Ga-FAPI for thyroid cancer, this study aims to focus specifically on the role of [⁶⁸Ga]Ga-DOTA.SA.FAPi imaging in patients with thyroid cancer who have the worst outcomes and are resistant to radioiodine. The study also aims to compare the diagnostic performance of [⁶⁸Ga]Ga-DOTA.SA.FAPi and [¹⁸F]F-FDG PET/CT in patients with radioiodine-resistant follicular-cell derived thyroid cancer.

Materials and methods

The retrospective study conducted in this research received approval from the institute ethics committee at All India Institute of Medical Sciences, New Delhi, India. Patient enrollment took place from April 2019 to October 2022. The study involved a collaboration between the Department

of Nuclear Medicine and the Medical Oncology Department at All India Institute of Medical Sciences, along with the Department of Chemistry at Johannes Gutenberg University, Mainz, Germany. The labeling precursor used in the study was provided by the Department of Chemistry, as shown in Fig. 1.

Synthesis of [^{68}Ga]Ga-DOTA.SA.FAPi and quality control

Radiolabeling of [^{68}Ga]Ga-DOTA.SA.FAPi was conducted as detailed in our previous publications [18] and detailed in supplementary data.

Definition of radioiodine-resistant thyroid cancer (RAI-R-FCTC)

Radioiodine-resistant follicular-cell derived thyroid cancer (RAI-R-FCTC) encompasses various scenarios indicating a loss of thyroid differentiation features or a lack of response to radioiodine treatment. These scenarios include follicular-cell derived thyroid cancer that shows negative results on a radioiodine whole body scan, metastatic DTC (RR-DTC) that continues to progress despite radioiodine uptake, persistent disease in DTC patients even after receiving a cumulative dose of I-131 exceeding 22.2GBq (600 mCi), the presence of one or more lesions that do not demonstrate radioactive iodine uptake, the development of de novo radioiodine refractory disease, and a combination of FDG-positive, elevated thyroglobulin, and I-131-negative lesions, known as TENIS syndrome.

The study enrolled patients who met specific eligibility criteria, which included the following: patients with histologically confirmed thyroid cancer derived from follicular cells, patients with radioiodine refractory follicular-cell derived thyroid cancer (RAI-R-FCTC), patients who underwent both [^{18}F]F-FDG and [^{68}Ga]Ga-DOTA.SA.FAPi PET/CT scans within a one-month interval, and patients who provided written informed consent. Pregnant and lactating women were excluded from the study to ensure their safety.

In this study, a total of 163 potentially eligible patients were initially identified and approached for screening. However, 12 patients refused to undergo two PET/CT

scans, leaving 151 patients who were confirmed as eligible for further assessment. From this group, 34 subjects were excluded due to various reasons, including a time interval of more than 1 month between the two PET/CT scans for 16 patients, unavailability of histopathological examination (HPE) confirmation for 4 patients, and identification of 14 patients as non-radioiodine refractory follicular-cell derived thyroid cancer (non-RAI-R-FCTC). Ultimately, a total of 117 patients were included in the final analysis of the study (Fig. 2).

Patients in the study underwent specific preparations and procedures for the [^{18}F]F-FDG and [^{68}Ga]Ga-DOTA.SA.FAPi PET/CT scans. Before the [^{18}F]F-FDG injection, patients fasted for a minimum of 6 h, and their peripheral blood glucose levels were measured to ensure they were within normal range. The mean activities of the injected radiotracers were 270 MBq (range: 185 to 370 MBq) for [^{18}F]F-FDG and 180 MBq (range: 59.2 to 321 MBq) for [^{68}Ga]Ga-DOTA.SA.FAPi. Scans were acquired using a 128-slice GE Discovery 710 PET/CT scanner. The details of acquisition and processing are mentioned in supplementary materials. The assessment of the scans involved qualitative and quantitative evaluations. Qualitative assessment compared patient-based and lesion-based visual interpretations, considering any lesion with higher uptake than the surrounding background tissue as positive. The quantitative assessment involved calculating standardized uptake values corrected for lean body mass (SULpeak and SULavg). Median SUV values were recorded for each site for both [^{18}F]F-FDG and [^{68}Ga]Ga-DOTA.SA.FAPi. The average SUV values of the three lesions with the highest uptake were calculated for each organ. To establish a reference standard, a combination of diagnostic CT scans, histological examination (when feasible), and/or clinico-radiological follow-up was utilized. Usually, local disease, nodal, and liver metastases could be targeted for histological confirmation, while lung and skeletal metastases were confirmed on diagnostic CT. Due to the presence of primary tumor and nodal metastases with concurrent distant metastatic involvement, no locoregional surgery was performed for these patients. All patients with primary residual tumor and lymph node metastases underwent histopathological confirmation.

Fig. 1 Chemical structure of the labeling precursor DOTA.SA.FAPi

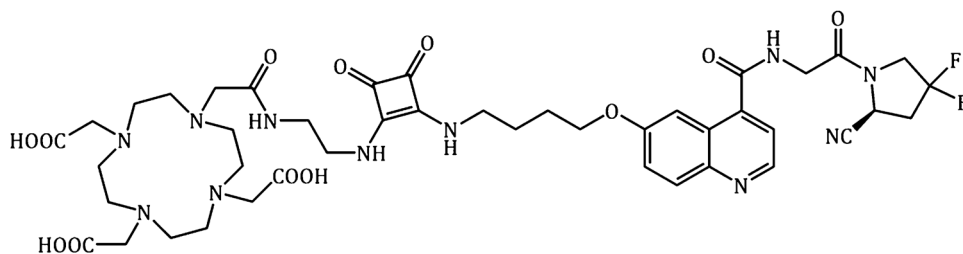
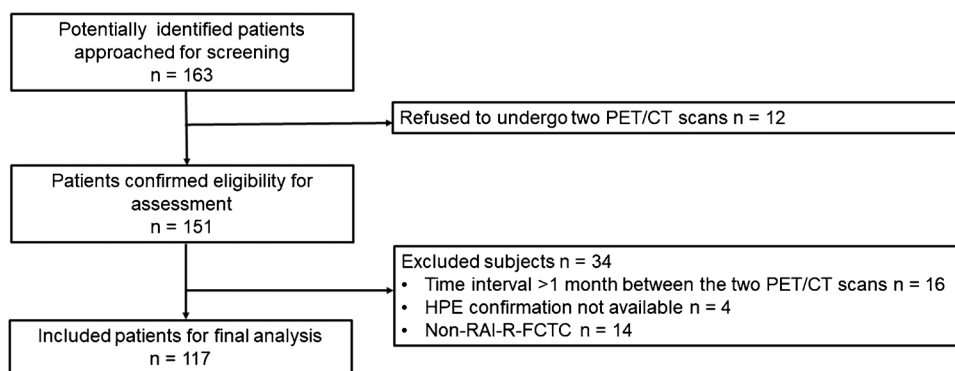


Fig. 2 Flowchart depicting the selection strategy of patients



Definitions

- True-positive (TP) lesion: active uptake in the lesion seen on [^{18}F]F-FDG/[^{68}Ga]Ga-DOTA.SA.FAPiPET/CT images and found to be positive on diagnostic CT/histological examination.
- False-positive (FP) lesion: active uptake in the lesion seen on [^{18}F]F-FDG/[^{68}Ga]Ga-DOTA.SA.FAPiPET/CT images and found to be negative on diagnostic CT/ histological examination/clinical or radiological follow-up.
- True-negative (TN) lesion: no uptake seen on [^{18}F]F-FDG/[^{68}Ga]Ga-DOTA.SA.FAPi PET/CT images and the results on diagnostic CT/histological examination/clinical or radiological follow-up were also negative.
- False-negative (FN) lesion: a lesion that was missed in [^{18}F]F-FDG / [^{68}Ga]Ga-DOTA.SA.FAPi PET/CT images but were found to be positive for malignancy at diagnostic CT/histological examination/clinical or radiological follow-up.

Statistical analysis

Categorical variables were expressed as numbers and percentages. Continuous variables were presented in terms of mean, median, standard deviation (SD), range, and interquartile range (IQR). [^{18}F]F-FDG and [^{68}Ga]Ga-DOTA.SA.FAPi uptake values were compared using paired Wilcoxon signed-rank test. Statistical differences in the detection rates of local disease, lymph nodal, and distant metastases between [^{18}F]F-FDG and [^{68}Ga]Ga-DOTA.SA.FAPi scans were analyzed by the McNemar test. Statistical analysis was performed using MedCalc statistical software.

Results

Table 1 presents the patient demographics and clinical parameters of a study involving 117 individuals. The key findings are as follows: the mean age of the patients was

53.2 years. Among the participants, 42% were male, while 58% were female. Regarding primary treatment, 11% of the patients underwent only total thyroidectomy, 84% received total thyroidectomy along with nodal dissection, and 5% were deemed inoperable. The study investigated various subtypes of radioiodine resistance. Among the participants, 18.8% experienced radiological disease progression despite radioiodine uptake, 32.5% had persistent disease in differentiated thyroid cancer (DTC) despite receiving a cumulative I-131 dose greater than 22.2 GBq (600 mCi), 12.8% had lesions that did not demonstrate radioactive iodine uptake, 15.4% had de novo radioiodine refractory disease, and 20.5% had a combination of [^{18}F]F-FDG positive, elevated thyroglobulin, and I-131 negative lesions (TENIS syndrome). The median cumulative activity of I-131 administered to the patients was 28.5 GBq, with an interquartile range (IQR) spanning from 13.6 to 40 GBq. Tyrosine kinase inhibitors were utilized as a treatment option in the majority of cases (92%), with 36% of patients receiving a single line of treatment and 56% undergoing two or more lines. External beam radiation therapy was administered to 41% of the patients. The primary site of the disease was the neck in 10% of cases, while 31% of patients presented with metastatic sites. The baseline median thyroglobulin values were measured at 183 ng/mL, with an IQR of 8.9 to 297 ng/mL. Eighty-six (73.5%) patients had RR-DTC disease, and the remaining thirty-one (26.5%) patients had poorly differentiated thyroid cancer (Table 2).

Following the intravenous injection of [^{68}Ga]Ga-DOTA.SA.FAPi, there were no observed adverse events, and all vital parameters remained within normal ranges.

Comparison of lesion detection and uptake between [^{18}F]F-FDG and [^{68}Ga]Ga-DOTA.SA.FAPi PET/CT scans

Local tumor

Out of the 117 patients included in the study, 60 had unilateral local disease, while 9 had bilateral lesions. It was found that there was complete concordance in the detection rate between

Table 1 Patient demographics and clinical parameters

Parameters	Values (N = 117)
Age in years (mean ± SD)	53.2 ± 11.7
Gender	
Male	49 (42%)
Female	68 (58%)
Primary treatment	
Total thyroidectomy	13 (11%)
Total thyroidectomy + nodal dissection	98 (84%)
Inoperable	6 (5%)
Radioiodine-resistant subtypes	
Radiological disease progression despite radioiodine uptake	22 (18.8%)
Persistent disease in DTC patients despite cumulative I-131 of >22.2GBq (600 mCi)	38 (32.5%)
One or more lesions did not demonstrate radioactive iodine uptake	15 (12.8%)
De novo radioiodine refractory disease	18 (15.4%)
Combination of [¹⁸ F]F-FDG positive, elevated thyroglobulin, and I-131 negative lesions (TENIS syndrome)	24 (20.5%)
Median I-131 cumulative activity (GBq) (IQR)	28.5 (13.6 to 40)
Tyrosine kinase inhibitors	108 (92%)
One line	42 (36%)
≥Two lines	66 (56%)
External beam radiation therapy	48 (41%)
Primary site (neck)	12 (10%)
Metastatic site	36 (31%)
Baseline median thyroglobulin values (ng/mL) (median, 25–75% IQR)	183 (8.9–297)

Table 2 The detailed histopathology of the types of RAI-R-FCTC

HPE of thyroid cancer	Number of patients (n=117)
RR-DTC	86 (73.5%)
Classic PTC	53 (45.30%)
FVPTC	13 (11.0%)
Tall cell variant PTC	3 (2.56%)
FTC	17 (14.5%)
PDTC*	31 (26.5%)

PTC papillary thyroid cancer; FVPTC follicular variant of papillary thyroid carcinoma; FTC follicular thyroid carcinoma; PDTC poorly differentiated thyroid cancer. *Differentiated component is present

both radiotracers, as indicated in Table 3. The median SUL values were also comparable between the tracers {SUL_{peak} [⁶⁸Ga]Ga-DOTA.SA.FAPi: 10.82; (IQR: 5.11 to 22.2), vs [¹⁸F]F-FDG: 7.86; (IQR: 4.15 to 20.84, p=0.263)} (Table 4).

Lymph node metastases

Out of 117 patients, a total of 537 lymph node (LN) metastases were identified on computed tomography (CT) in 99 patients (84.6%). The comparison between [⁶⁸Ga]Ga-DOTA.SA.FAPi and [¹⁸F]F-FDG in detecting LN metastases showed that [⁶⁸Ga]

Ga-DOTA.SA.FAPi detected 95.4% (512/537) of LN metastases, while [¹⁸F]F-FDG detected 86.8% (465/537). This difference in detection rates was found to be statistically significant ($p < 0.0001$). The specific breakdown of the results showed that [⁶⁸Ga]Ga-DOTA.SA.FAPi had 467 true positives (TP), 16 true negatives (TN), 4 false positives (FP), and 25 false negatives (FN) in detecting LN metastases. On the other hand, [¹⁸F]F-FDG had 432 TP, 16 TN, 17 FP, and 72 FN. The lower number of false positives that was observed with [⁶⁸Ga]Ga-DOTA.SA.FAPi (4/512, 0.8%) compared to [¹⁸F]F-FDG (17/465, 3.7%) was found to be statistically significant ($p < 0.0001$). The difference in the detection rates of LN metastases between [⁶⁸Ga]Ga-DOTA.SA.FAPi and [¹⁸F]F-FDG were calculated to be 8.7% (95% CI: 2.77–7.15%), with a chi-square value of 24.1% ($p < 0.0001$). Furthermore, there was no significant difference in the SUL_{peak} values of the LN metastases between the two radiotracers. The SUV_{max} values for [⁶⁸Ga]Ga-DOTA.SA.FAPi and [¹⁸F]F-FDG were 6.86 (3.21 to 12.72) and 5.018 (2 to 10.17), respectively, and the p -value was 0.286 (Tables 3 and 4).

Lung metastases

Eighty-two patients (70%) were diagnosed with lung metastasis on CT imaging. The [⁶⁸Ga]Ga-DOTA.SA.FAPi scan demonstrated concordant findings in 67 (81.7%) of these patients, while [¹⁸F]F-FDG showed complete

Table 3 Comparison of detection efficiency: [⁶⁸Ga]Ga-DOTA.SA.FAPi versus [¹⁸F]F-FDG in patient-based and lesion-based analyses

Parameters	Imaging method	Primary	Lymph node metastasis	Lung metastasis	Pleural thickening	Liver metastases	Bone metastases	Brain metastases
Patient-based analysis								
	CT	69	99	82	11	30	53	11
	[⁶⁸ Ga]Ga-DOTA.SA.FAPi	69 (100%)	85 (86%)	67 (81.7%)	11 (100%)	30 (100%)	53 (100%)	11 (100%)
	[¹⁸ F]F-FDG	69 (100%)	76 (77%)	53 (64.6%)	11 (100%)	27 (90%)	53 (100%)	9 (81.80%)
	<i>p</i> -value	1.000	0.147	0.020	1.000	0.236	1.000	0.457
Lesion-based analysis								
	CT	78	537	NA	11	107	NA	23
	[⁶⁸ Ga]Ga-DOTA.SA.FAPi	78 (100%)	512 (95.4%)	NA	11 (100%)	107 (100%)	NA	23 (100%)
	[¹⁸ F]F-FDG	78 (100%)	465 (86.8%)	NA	11 (100%)	87 (81.3%)	NA	9 (39%)
	<i>p</i> -value	1.000	<0.0001	NA	1.000	<0.0001	NA	<0.0001

NA not assessed

Table 4 Comparison between [⁶⁸Ga]Ga-DOTA.SA.FAPi and [¹⁸F]F-FDG standardized uptake values in various locations of metastasis

Location of primary/metastasis	No. of patients	No. of primary/metastasis	[⁶⁸ Ga]Ga-DOTA.SA.FAPi (SULpeak)	[¹⁸ F]F-FDG (SULpeak)	<i>p</i> -value	[⁶⁸ Ga]Ga-DOTA.SA.FAPi (SULavg)	[¹⁸ F]F-FDG (SULavg)	<i>p</i> -value
Thyroid remnant	69 (60%)	78	10.82 [5.11 to 22.2]	7.86 [4.15 to 20.84]	0.263	5.91 [2.80 to 7.99]	3.76 [1.84 to 15.28]	0.167
Lymph nodes	99 (84.61%)	537	6.86 [3.21 to 12.72]	5.018 [2 to 10.17]	0.286	3.42 [2.02 to 6.28]	2.05 [1.01 to 6.32]	0.1931
Lung metastasis	82 (70.08%)	-	5.64 [2.23 to 10.95]	4.96 [2.11 to 10.22]	0.4274	3.60 [1.25 to 7.25]	3.63 [1.88 to 5.77]	0.9589
Bone metastasis	53 (45.3%)	<6 sites <i>n</i> = 14 6–20 <i>n</i> = 31 >20 <i>n</i> = 8	8.24 [5.62 to 14.82]	6.9 [3.17 to 13.1]	0.1830	4.22 [2.48 to 7.51]	3.47 [1.97 to 7.39]	0.2424
Liver metastasis	30 (25.6%)	107	7.28 [4.82 to 12.31]	5.97 [3.01 to 7.95]	0.212	4.01 [2.80 to 7.2]	2.16 [1.38 to 3.37]	0.1016
Brain metastasis	11 (9.4%)	23	13.9 [6.89 to 28.71]	6.7 [2.24 to 9.23]	0.0001	6.89 [2.1 to 9.23]	3.23 [1.1 to 6.72]	0.0001
Pleural metastasis	11 (9.4%)	-	5.82 [3.2 to 8.6]	6.45 [2.13 to 10.1]	0.486	2.63 [1.86 to 4.16]	3.1 [1.33 to 6.22]	0.534
Muscle metastasis	3 (2.5%)	6	9.56 [8.32 to 12.06]	5.62 [4.9 to 6.89]	0.0085	6.1 [4.86 to 8.61]	3.33 [2.92–4.28]	0.0266
Bowel metastasis	1 (0.8%)	2	-	-	-	-	-	-

No. number

concordance in 53 (64.6%) patients (Table 3). Upon detailed analysis, [⁶⁸Ga]Ga-DOTA.SA.FAPi failed to show expression in 11 (13.4%) patients and exhibited a mixed uptake pattern (true positive + false negative) in 4 patients.

Eleven patients showed no FDG uptake (true negative) on [¹⁸F]F-FDG scans. In addition, a mixed uptake pattern, consisting of both true-positive and false-positive results, was observed in 18 patients (true positive + true negative + false positive). Interestingly, a complete discordance in radiotracer uptake was noted in cases where [⁶⁸Ga]Ga-DOTA.SA.FAPi, in accordance with the CT scan findings, demonstrated no uptake in the lung lesions. However, false-positive uptake was observed on [¹⁸F]F-FDG scans in seven patients, which corresponded to infective

sequelae (as depicted in Fig. 3). Notably, in five patients with radiologically detected lung metastases, both [⁶⁸Ga]Ga-DOTA.SA.FAPi and [¹⁸F]F-FDG scans showed no activity of the radiotracers. Among these cases, four patients had radioiodine-resistant differentiated thyroid cancer (RR-DTC), and one patient had poorly differentiated histology.

Bone metastases

The bone lesions were categorized based on the number of bone metastases. Out of the 53 (45.3%) patients with bone metastases, fourteen patients had fewer than 6 bone metastases, 31 patients had between 6 and 20 bone metastases, and eight patients had more than 20 bone metastases. Both

radiotracers demonstrated complete agreement in detecting bone metastases, and similar uptake values were observed between the two radiotracers {SULpeak: 8.24 [5.62 to 14.82] vs. 6.9 [3.17 to 13.1], $p=0.1830$ } (Tables 3 and 4).

Liver metastases

Among the thirty patients with liver metastases, a total of 107 liver metastases were detected. ^{68}Ga]Ga-DOTA.SA.FAPi accurately identified all the liver metastases (Table 3). In contrast, ^{18}F]F-FDG could only detect 87 (81.3%) of the liver lesions, with a complete failure to detect any liver metastases in three patients (Figs. 4 and 5). Significantly discordant findings were observed in the poorly differentiated category, where ^{68}Ga]Ga-DOTA.SA.FAPi detected all forty-six liver metastases, while ^{18}F]F-FDG could only detect twenty-one ($p<0.0001$).

Figure 4 depicts an interesting case of a 66-year-old female with poorly differentiated thyroid carcinoma who underwent ^{18}F]F-FDG PET/CT for follow-up. The ^{18}F]F-FDG PET/CT images showed minimal uptake in the bilateral lung metastases and no abnormal findings in other organs (Fig. 4A). However, axial sections from the CT scan revealed bilateral lung nodules and liver metastases (Fig. 4B). To further evaluate the case, ^{68}Ga]Ga-DOTA.SA.FAPi PET/CT was performed, which demonstrated intense uptake in the bilateral lung nodules and multiple liver lesions (Fig. 4C). The addition of ^{68}Ga]Ga-DOTA.SA.FAPi improved the detection of metastases in the lung and liver.

Another noteworthy instance (Fig. 5) illustrates the added value of utilizing both ^{18}F]F-FDG PET/CT and ^{68}Ga]Ga-DOTA.SA.FAPi imaging is as follows: a 65-year-old female with RR-DTC exhibited intense uptake of ^{18}F]F-FDG in mediastinal lymph nodes, which was practically non-existent on ^{68}Ga]Ga-DOTA.SA.FAPi PET/CT. Conversely, the patient displayed remarkable ^{68}Ga]Ga-DOTA.SA.FAPi accumulation in bilateral lung nodules, liver, and pelvic bone metastases. By employing a complementary dual scan approach, the diagnostic performance significantly improved in this particular case, as it encompassed instances of true-positive, false-positive, true-negative, and false-negative findings on both scans.

Other distant metastases

Pleural metastases were detected in eleven patients, and both radiotracers showed similar detection rates and uptake patterns for these metastases. In one patient, a bowel metastasis was missed on the ^{18}F]F-FDG scan due to physiological interference but was successfully delineated on the ^{68}Ga]Ga-DOTA.SA.FAPi scan. Muscle metastases were observed in three patients, with a total of six sites detected on both scans. The uptake on the ^{68}Ga]Ga-DOTA.SA.FAPi scan was found to be higher than that of ^{18}F]F-FDG for these muscle metastases.

A total of 23 brain metastases were identified in eleven patients. Strikingly, two patients had brain metastases that

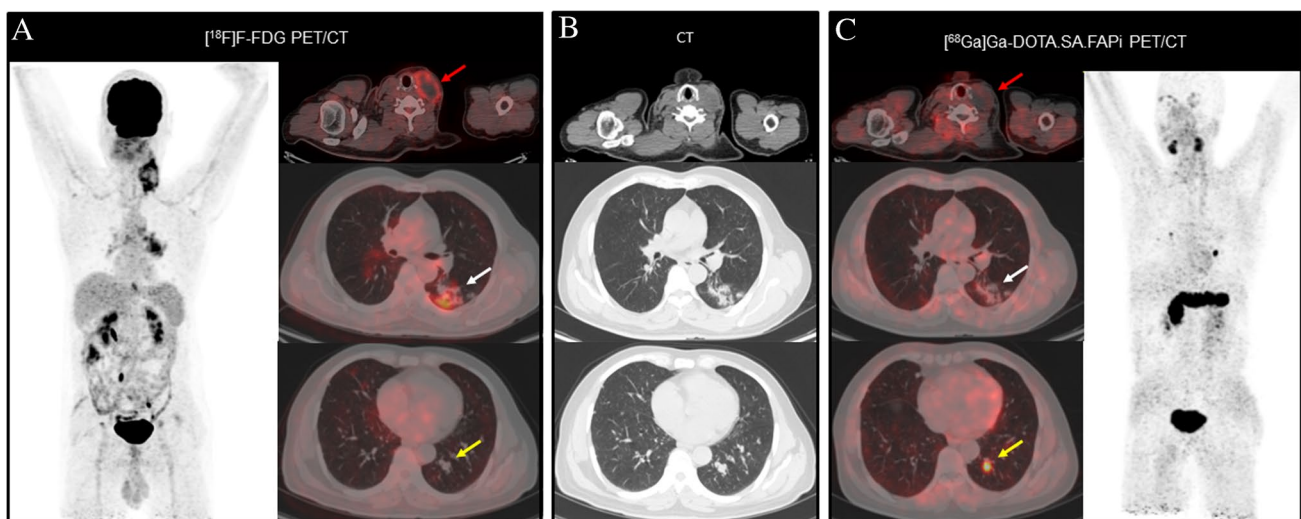


Fig. 3 In a 75-year-old male patient with poorly differentiated carcinoma and a mixed component of anaplastic thyroid carcinoma, peripheral ^{18}F]F-FDG avidity is noted in a large left level III/IV cervical lymph nodal mass measuring 5.4×5.2 cm [SULpeak: 5.8] (A, red arrow). Multiple sub-centimetric sized bilateral lung nodules were noted with no ^{18}F]F-FDG avidity (A, yellow arrow). Fibrotic

changes with intense FDG avidity in the left lung (A (white arrow) and (B, middle row) is an infective sequelae. On the other hand, ^{68}Ga]Ga-DOTA.SA.FAPi did not demonstrate any uptake in the lymph node (C, red arrow) but demonstrated intense FAPi expression in the lung metastases [SUL peak: 4.2] (C, yellow arrow) and no uptake in the corresponding left lung fibrotic mass (C, white arrow)

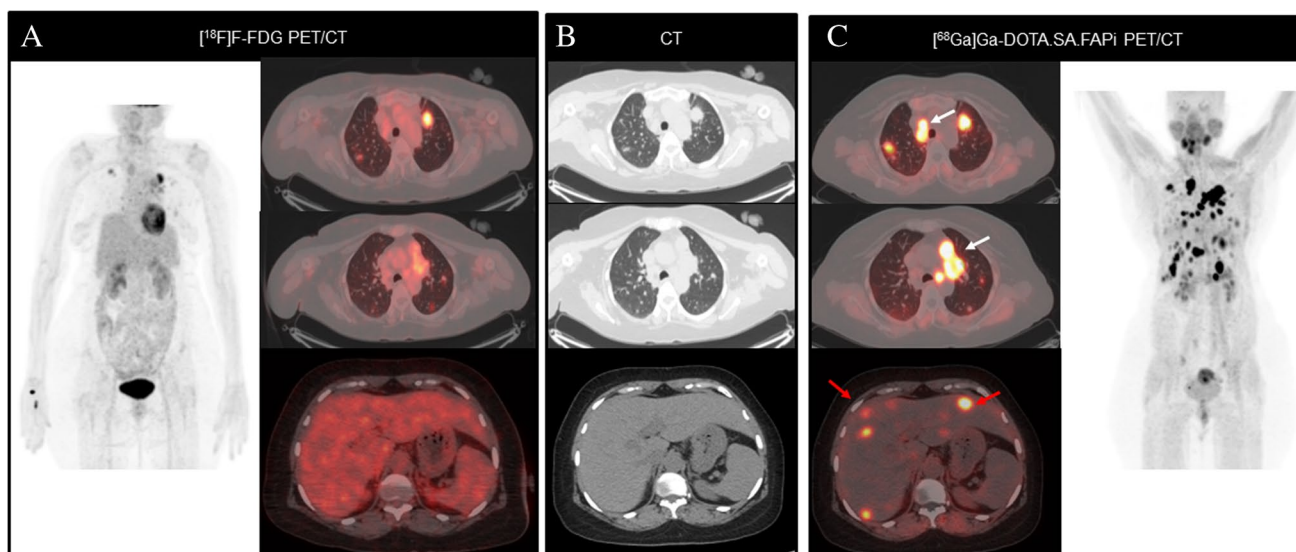


Fig. 4 A 66-year-old female was diagnosed with poorly differentiated thyroid carcinoma with an anaplastic component and underwent $[^{18}\text{F}]\text{F-FDG}$ PET/CT for follow-up. **A** Images from the $[^{18}\text{F}]\text{F-FDG}$ PET/CT scan demonstrate minimal $[^{18}\text{F}]\text{F-FDG}$ uptake in the bilateral lung metastases [SUL peak: 2.8] and normal findings in the rest

of the organs. **B** CT scan axial sections reveal bilateral lung nodules and liver metastases. **C** $[^{68}\text{Ga}]\text{Ga-DOTA.SA.FAPi}$ PET/CT was performed for further evaluation, and scan findings revealed intense uptake in bilateral lung nodules [SULpeak: 7.8] (**C**, white arrows) and multiple liver lesions [SULpeak: 6.9] (**C**, red arrows)

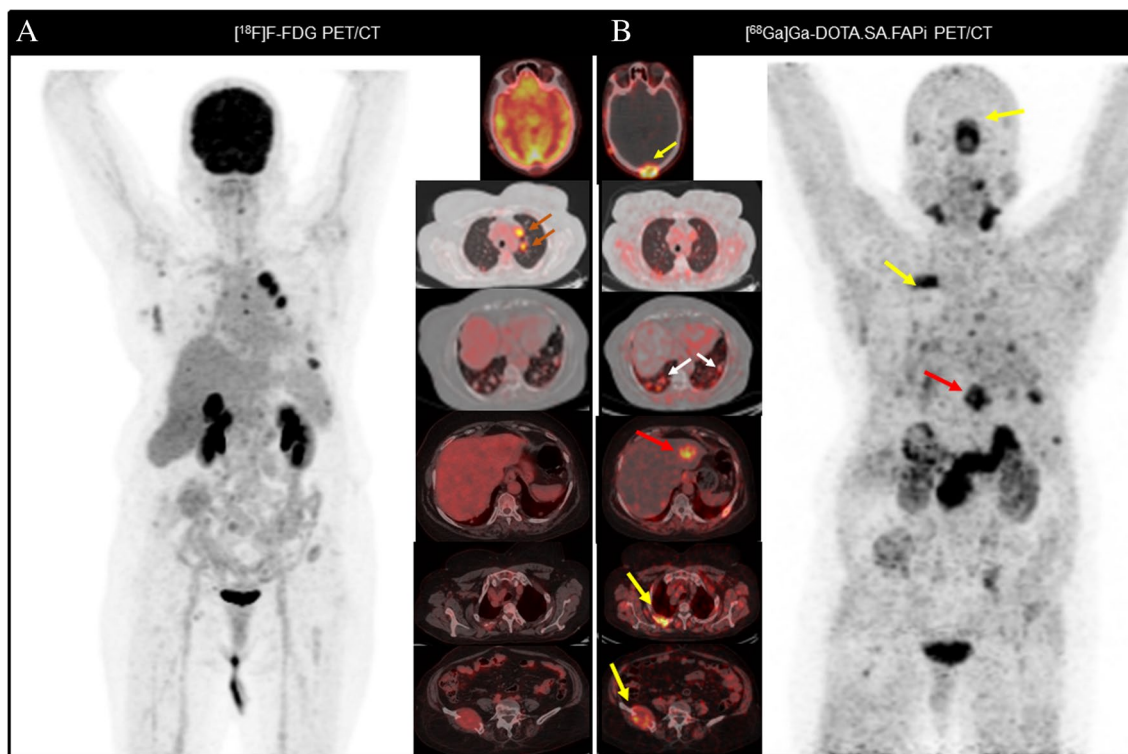


Fig. 5 In a 65-year-old female with RR-DTC (HPE: follicular variant of papillary thyroid cancer), **A** $[^{18}\text{F}]\text{F-FDG}$ PET MIP image demonstrated intense $[^{18}\text{F}]\text{F-FDG}$ uptake in the mediastinal LNs [SULpeak: 7.6] (MIP and CT axial (**A**, orange arrows)) which was negligible on $[^{68}\text{Ga}]\text{Ga-DOTA.SA.FAPi}$ PET/CT [SULpeak: 1.8]. On the contrary,

$[^{68}\text{Ga}]\text{Ga-DOTA.SA.FAPi}$ PET/CT (**B**, **C**) demonstrated additional FAPi expression in the bilateral lung nodules [SULpeak: 2.6] (white arrows **B**), liver [SULpeak: 5.4] (red arrows **B**, **C**), and bone metastases [SULpeak: 5.2] (yellow arrows **B**, **C**) that did not show $[^{18}\text{F}]\text{F-FDG}$ uptake

were completely missed on the [^{18}F]F-FDG PET/CT scans. In contrast, the [^{68}Ga]Ga-DOTA.SA.FAPi scan achieved a remarkable 100% detection rate for brain metastases, which was significantly higher than the 39% (9/23) detection rate achieved by [^{18}F]F-FDG PET/CT ($p < 0.0001$) (Table 3).

Additionally, the standardized uptake value (SUL) derived from the [^{68}Ga]Ga-DOTA.SA.FAPi scan exhibited a noteworthy distinction compared to [^{18}F]F-FDG in brain metastases. The [^{68}Ga]Ga-DOTA.SA.FAPi-derived SUL values were approximately twofold higher than those of [^{18}F]F-FDG. Specifically, the SUL peak values for [^{68}Ga]Ga-DOTA.SA.FAPi and [^{18}F]F-FDG in brain metastases were 13.9 (6.89 to 28.7) and 6.7 (2.24 to 9.23), respectively. This difference was statistically significant ($p < 0.0001$) (Table 4).

Discussion

Theranostic options for aggressive thyroid cancer patients become limited after radioiodine therapy is exhausted. However, in recent years, radiopharmaceuticals utilizing fibroblast activation protein inhibitors have emerged as potential theranostic agents for thyroid cancer, marking a significant development in the field nearly eight decades after the introduction of radioiodine.

In this study, we aimed to compare the diagnostic performance of [^{68}Ga]Ga-DOTA.SA.FAPi with [^{18}F]F-FDG PET/CT in patients with radioactive iodine refractory follicular-cell derived thyroid carcinomas (RAI-R-FCTCs). The primary objective was to systematically evaluate the differences between FAPi expression and glucose uptake in the detection of RAI-R-FCTC. The results of the study demonstrated that [^{68}Ga]Ga-DOTA.SA.FAPi had a higher detection rate for lymph nodes (95.4% vs. 86.8%, $p < 0.0001$), liver metastases (100% vs. 81.3%, $p < 0.0001$), and brain metastases (100% vs. 39%, $p < 0.0001$) compared to [^{18}F]F-FDG PET/CT. These findings indicate that [^{68}Ga]Ga-DOTA.SA.FAPi outperformed [^{18}F]F-FDG PET/CT in terms of detecting a greater number of lymph nodes, liver metastases, and brain metastases in patients with RAI-R-FCTC. Further, a remarkable concordance was observed in the detection of the local tumor, pleural metastases, and skeletal metastases. This concordance indicates a consistent and reliable ability of the imaging modalities used to identify these specific sites of metastasis in thyroid cancer.

In our study, we observed that the semi-quantitative parameters, such as SUL peak (standardized uptake value peak) and average values, were similar between the two radiotracers for various metastatic sites. However, [^{68}Ga]Ga-DOTA.SA.FAPi exhibited substantially higher values for brain and muscle metastases compared to [^{18}F]F-FDG.

Additionally, several studies have reported a favorable property of [^{68}Ga]Ga-FAPi PET scans, regardless of the specific FAPi molecule used. These studies have indicated that [^{68}Ga]Ga-FAPi PET scans show low uptake in normal parenchyma, which is advantageous for tumor delineation, particularly in regions such as the head and neck and liver, across different types of cancers [20–22]. Likewise, our findings also suggest that [^{68}Ga]Ga-DOTA.SA.FAPi has a distinct advantage in terms of higher uptake values for brain and muscle metastases compared to [^{18}F]F-FDG.

Lymph node (LN) metastasis in the locoregional area is often an initial site of disease progression in thyroid cancer before spreading to distant organs. However, the diagnosis of central compartment LN metastases using ultrasonography is limited due to the deep location of certain LNs around the trachea and overlapping structures, resulting in false-negative results. Currently, [^{18}F]F-FDG PET/CT is the preferred imaging modality for evaluating radioactive iodine refractory differentiated thyroid cancer (RR-DTC) and other aggressive variants like Hürthle, insular, poorly differentiated thyroid carcinoma (PDTC), and anaplastic thyroid carcinoma (ATC). However, its clinical utility is hindered by its high false-positive rates caused by inflammatory lymphadenopathy. Our study demonstrated that [^{68}Ga]Ga-DOTA.SA.FAPi PET/CT showed superior reliability in detecting lymph node metastases compared to [^{18}F]F-FDG PET/CT (Table 3). These findings align with previous research conducted by Wang et al. [22]. They reported that [^{68}Ga]Ga-FAPi PET/CT imaging has the potential to detect lymph node metastases at an earlier stage and enhance the identification of occult lymph node metastasis, thereby enabling more accurate staging of thyroid cancer patients.

The sensitivity of [^{18}F]F-FDG for detecting small metastatic lesions and its specificity for distinguishing infective lung pathology were relatively low. Similarly, [^{68}Ga]Ga-DOTA.SA.FAPi showed mixed uptake in lung metastases. Both radiotracers exhibited false-negative results in lung metastases, but [^{18}F]F-FDG had a higher percentage of false negatives compared to [^{68}Ga]Ga-FAPi. One possible explanation for this discrepancy is the rapid efflux of [^{18}F]F-FDG from tumor cells in highly aggressive metastases. Another factor could be the limited uptake or absence of uptake in lung metastases on both radiotracers, which could be influenced by the size of the lesions and breathing artifacts. Therefore, it is evident that a breath-hold CT scan accompanied by careful clinical follow-up remains crucial for diagnosing small lung nodules with uncertain uptake on both radiotracers. Further comprehensive studies are needed to investigate this uptake pattern in different subtypes of thyroid cancers.

The diagnosis and detection of poorly differentiated thyroid carcinoma (PDTC) have been a subject of controversy, both in terms of histopathological staging and imaging

methods. This lack of clarity has also made the management of PDTC challenging. While [^{18}F]F-FDG is widely accepted as the preferred imaging agent for radioactive iodine refractory differentiated thyroid carcinoma (RR-DTC), its role as the imaging modality of choice for PDTC has not been clearly defined by the American Thyroid Association (ATA). Nonetheless, FDG imaging has been extensively studied in relation to PDTC. Although PDTC tumors often exhibit high FDG uptake, some studies have indicated intermediate levels of GLUT1 expression and FDG uptake values between differentiated thyroid carcinoma (DTC) and anaplastic thyroid carcinoma (ATC) [23, 24]. The significantly higher detection rate of fibroblast activation protein inhibitor (FAPi) in PDTC, regardless of the presence of ATC component, compared to FDG imaging, has introduced a new imaging option for these aggressive variants. The varied uptake patterns and intermediate FDG expression observed in PDTC have generated conflicting results, but the consistent positive expression of FAPi in all PDTC lesions offers new possibilities for systemic treatment in patients who have limited treatment options.

Our study uncovered a notable finding regarding the expression of FAPi in highly aggressive tumors, specifically focusing on PDTC (Fig. 4). Emerging research has revealed a striking finding regarding highly aggressive tumors, which is their predominantly stromal composition of approximately 90% rather than being primarily composed of tumor cells. We observed higher levels of FAPi expression in these tumors, indicating its potential significance in their aggressive behavior. This combination of increased FAPi expression and a predominant stromal component provides valuable insights into the underlying biology and behavior of these tumors. It highlights the intricate interplay between tumor cells and the surrounding stromal environment, which can influence various aspects, including imaging results and the heterogeneous nature of tumor characteristics. The elevated expression of FAPi suggests its involvement in the aggressive phenotype of PDTC and possibly other highly aggressive tumors. The stromal-rich composition of these tumors, coupled with lower glycolytic activity, may contribute to the observed heterogeneity in imaging results. This finding underscores the importance of considering the tumor microenvironment, particularly the tumor stroma when interpreting imaging findings and comprehending the behavior of highly aggressive tumors such as PDTC. In summary, our study's identification of higher FAPi expression and the predominance of tumor stroma in highly aggressive tumors shed light on their underlying biology and behavior.

The role of different [^{68}Ga]Ga-labeled FAPi molecules in thyroid cancers has been investigated in a limited number of studies, and the results have been mixed. Some

studies have reported limited effectiveness of [^{68}Ga]Ga-DOTA.SA.FAPi in thyroid cancer cases with low radioiodine expression. These studies have shown low uptake of [^{68}Ga]Ga-labeled FAPi in radioiodine refractory differentiated thyroid cancer (RR-DTC). For instance, Kratochwil et al. [16] observed low uptake of [^{68}Ga]Ga-FAPi-04 in certain cancers, including differentiated thyroid cancer with a maximum standardized uptake value (SUVmax) of less than 6. Similarly, Giesel et al. [15] found that dedifferentiated thyroid cancer cases with a flip-flop pattern of [^{18}F]F-FDG uptake did not exhibit significant accumulation of [^{68}Ga]Ga-FAPi-04. Huang et al. [25] also reported low tracer uptake of [^{68}Ga]Ga-FAPi compared to [^{18}F]F-FDG PET in patients with iodine-negative thyroid cancer. Currently, [^{18}F]F-FDG PET/CT remains the preferred PET radiopharmaceutical for restaging purposes in thyroid cancer due to its wide availability, cost-effectiveness, and standardized quantification techniques. On the other hand, [^{68}Ga]Ga-FAPi can potentially play a complementary role in the field of theranostics. Notably, our recent study conducted on medullary thyroid cancer demonstrated the superiority of [^{68}Ga]Ga-FAPi over [^{68}Ga]Ga-DOTANOC imaging, representing a significant advancement in the field of theranostics for thyroid cancer [26].

The potential of [^{68}Ga]Ga-FAPi radiotracers for imaging purposes has been demonstrated; however, their therapeutic counterparts have shown rapid clearance from tumor sites. To overcome this limitation and enhance the therapeutic potential of FAPi-based compounds, Moon et al. conducted structural modifications and optimization of the monomeric FAPi precursor, resulting in the development of homodimeric compounds. These modified compounds exhibited prolonged retention time in tumors, as demonstrated in their study [19]. Subsequently, the same research group investigated the dosimetry and pharmacokinetics of [^{177}Lu]Lu-DOTAGA.(SA.FAPi)₂, a homodimeric compound, in patients with radioiodine-resistant differentiated thyroid cancer (RR-DTC). The study showed significant and prolonged tumor retention up to 168 h post-treatment [27]. However, it is important to note that the study only included RR-DTC patients, and further research should focus on expanding this treatment option to include a broader range of radioiodine-resistant thyroid cancers (RAI-R TC), including poorly differentiated thyroid cancer (PDTC) and anaplastic thyroid cancer (ATC). Assessing the long-term outcomes of [^{177}Lu]Lu-FAPi treatment in various types of thyroid cancer will provide a more accurate understanding of its utility as a treatment approach.

While the role of [^{68}Ga]Ga-FAPi in thyroid cancer imaging is still being explored, it currently serves as a complementary tool alongside [^{18}F]F-FDG PET/CT, offering potential advantages in specific cases and contributing to the progress of theranostics in thyroid cancer.

Limitations

Several limitations were identified in our study. Firstly, it should be noted that our study was a retrospective analysis, which may introduce inherent biases and limitations. Additionally, the majority of the included cases were classic radioactive iodine refractory differentiated thyroid carcinomas (RR-DTC), with smaller sample sizes for other non-iodine concentrating thyroid cancer histological subtypes. This limited representation of histological subtypes reduces the generalizability of our findings and calls for larger sample sizes and well-executed clinical trials with strict eligibility criteria to provide more robust evidence. Another limitation is that contrast-enhanced computed tomography (CECT) scans were not available for all patients in the study, which could have provided additional information for comparison and validation of the imaging findings. Moreover, the lack of gold-standard histopathological validation for all discrepant lesions is a limitation. Due to practical constraints, it was not feasible to obtain a biopsy from each lesion, which could have provided definitive confirmation of the imaging findings. Lastly, we were unable to assess the correlation between tumor mutation status, the microenvironment of thyroid cancer, and their impact on the uptake of both radiotracers. This information could have provided valuable insights into the underlying biological mechanisms influencing the imaging results. Considering these limitations, it is important to interpret the results of our study with caution and recognize the need for further research with larger and more diverse patient populations, prospective study designs, and comprehensive validation methods to strengthen the evidence and address these limitations effectively.

Conclusion

In this study, we conducted a comparison between the PET tracer [^{68}Ga]Ga-DOTA.SA.FAPi, which is a highly selective FAP inhibitor, and [^{18}F]F-FDG in patients with radioactive iodine refractory follicular-cell derived thyroid carcinomas (RAI-R-FCTCs). [^{68}Ga]Ga-DOTA.SA.FAPi demonstrated minimal physiological uptake, increasing the likelihood of detecting lymph node, hepatic, and brain metastases. Overall, [^{68}Ga]Ga-DOTA.SA.FAPi PET/CT demonstrated lower false-positive and false-negative rates as compared to [^{18}F]F-FDG. However, the prevalence of false positives and false negatives in both scans unfolds the necessity of a complementary dual scan approach to staging/restaging any thyroid cancer. Unlike [^{18}F]F-FDG, which is primarily used for imaging, the high selectivity of [^{68}Ga]Ga-DOTA.SA.FAPi for tumors holds promise for precision treatment in various FAPi-positive cancers. This finding opens avenues for future

research investigating the role of [^{68}Ga]Ga-DOTA.SA.FAPi PET/CT-guided treatment with radiolabeled agents such as [^{177}Lu] ^{90}Y / ^{225}Ac -FAPi in aggressive dedifferentiated variants of thyroid cancer, especially when no options for targeted kinase inhibitors (TKIs) are available. Overall, our study underscores the potential of [^{68}Ga]Ga-DOTA.SA.FAPi PET/CT as a valuable tool for the diagnosis and guiding targeted therapies in thyroid cancers. Future investigations in this area may pave the way for personalized and more effective treatment strategies in patients with RAI-R-FCTCs.

Supplementary Information The online version contains supplementary material available at <https://doi.org/10.1007/s00259-023-06404-z>.

Author contribution The study's conception and design involved contributions from all authors. Sanjana Ballal, Madhav Prasad Yadav, Nicky Wakade, Parvind Sheokand, Swayamjeet Satapathy, and Kunal R. Chandekar were responsible for material preparation, data collection, and analysis. The initial draft of the manuscript was written by Sanjana Ballal and Madhav Prasad Yadav. Chandrasekhar Bal and Madhavi Tripathi processed and reported the images, while Shipra Agarwal reviewed the pathology reports. Dr. Ranjit Kumar Sahoo and Dr. Sameer Rastogi referred patients for scans. Our collaborators from the University of Mainz, Frank Roesch, Euy Sung Moon, and Marcel Martin, synthesized the precursor and provided valuable input to finalize the manuscript. All authors provided feedback on earlier versions of the manuscript and approved the final version.

Data availability The datasets generated during and/or analyzed during the current study are available from the corresponding author upon reasonable request.

Declarations

Ethical approval Ethical clearance received Ref No: IECPG:22/27

Consent to participate Written informed consent was obtained from all patients to participate in the study, use clinical information to analyze data, and use images for the purpose of publication.

Conflict of interest The authors declare no competing interests.

Disclaimer This work has not been submitted elsewhere as a full article and is not under consideration by any other journal.

References


- Zarnegar R, Brunaud L, Kanauchi H, et al. Increasing the effectiveness of radioactive iodine therapy in the treatment of thyroid cancer using trichostatin A, a histone deacetylase inhibitor. *Surgery*. 2002;132:984–90.
- Dralle H, Machens A, Basa J, Fatourech V, Franceschi S, Hay ID, et al. Follicular cell-derived thyroid cancer. *Nat Rev Dis Primers*. 2015;10(1):15077.
- Worden F. Treatment strategies for radioactive iodine refractory differentiated thyroid cancer. *Ther Adv Med Oncol*. 2014;6:267–79.
- Xing M, Haugen BR, Schlumberger M. Progress in molecular-based management of differentiated thyroid cancer. *Lancet*. 2013;381:1058–69.
- Choudhury PS, Gupta M. Differentiated thyroid cancer theranostics: radioiodine and beyond. *Br J Radiol*. 2018;91:20180136.

6. Deandreis D, Ghuzlan A, Lebouilleux S, et al. Do histological, immunohistochemical, and metabolic (radioiodine and fluorodeoxyglucose uptakes) patterns of metastatic thyroid cancer correlate with patient outcome? *Endocr Relat Cancer*. 2011;18:159–69.
7. Rosenbaum-Krumme SJ GR, Bockisch A, et al. ¹⁸F-FDG PET/CT changes therapy management in high-risk DTC after first radioiodine therapy. *Eur J Nucl Med Mol Imaging*. 2012;39:1373–80.
8. Grewal RK, HoA SH. Novel approaches to thyroid cancer treatment and response assessment. *Semin Nucl Med*. 2016;46:109–18.
9. Klain M, Zampella E, Nappi C, et al. Advances in functional imaging of differentiated thyroid cancer. *Cancers*. 2021;13:4748.
10. Boellaard R, Delgado-Bolton R, Oyen WJ, et al. European Association of Nuclear Medicine (EANM) FDG PET/CT: EANM procedure guidelines for tumour imaging: version 2.0. *Eur J Nucl Med Mol Imaging*. 2015;42:328–54.
11. Fozzatti L, Cheng SY. Tumor cells and cancer-associated fibroblasts: a synergistic crosstalk to promote thyroid cancer. *Endocrinol Metab (Seoul)*. 2020;35:673–80.
12. Cho JG, Byeon HK, Oh KH, et al. Clinicopathological significance of cancer-associated fibroblasts in papillary thyroid carcinoma: a predictive marker of cervical lymph node metastasis. *Eur Arch Otorhinolaryngol*. 2018;275:2355–61.
13. Sun WY, Jung WH, Koo JS. 2016. Expression of cancer-associated fibroblast-related proteins in thyroid papillary carcinoma. *Tumour Biol*. 37:8197–8207.
14. Jansen K, Heirbaut L, Verkerk R, et al. Extended structure-activity relationship and pharmacokinetic investigation of (4-quinolinoyl) glycyL-2-cyanopyrrolidine inhibitors of fibroblast activation protein (FAP). *J Med Chem*. 2014;57:3053–74.
15. Giesel FL, Kratochwil C, Lindner T, et al. ⁶⁸Ga-FAPI PET/CT: biodistribution and preliminary dosimetry estimate of 2 DOTA-containing FAP-targeting agents in patients with various cancers. *J Nucl Med*. 2019;60:386–92.
16. Kratochwil C, Flechsig P, Lindner T, et al. ⁶⁸Ga-FAPI PET/CT: tracer uptake in 28 different kinds of cancer. *J Nucl Med*. 2019;60:801–5.
17. Meyer C, Dahlbom M, Lindner T, et al. Radiation dosimetry and biodistribution of ⁶⁸Ga-FAPI-46 PET imaging in cancer patients. *J Nucl Med*. 2020;61:1171–7.
18. Ballal S, Yadav MP, Moon ES, et al. Biodistribution, pharmacokinetics, dosimetry of [⁶⁸Ga]GaDOTA.SA.FAPi, and the head-to-head comparison with [¹⁸F]F-FDG PET/CT in patients with various cancers. *Eur J Nucl Med Mol Imaging*. 2021;48:1915–31.
19. Moon ES, Ballal S, Yadav MP, et al. Fibroblast activation protein (FAP) targeting homodimeric FAP inhibitor radiotheranostics: a step to improve tumor uptake and retention time. *Am J Nucl Med Mol Imaging*. 2021;11:476–91.
20. Pang Y, Zhao L, Luo Z, et al. Comparison of ⁶⁸Ga-FAPI and ¹⁸F-FDG uptake in gastric, duodenal, and colorectal cancers. *Radiology*. 2021;298:393–402.
21. Chen H, Pang Y, Wu J, et al. Comparison of [⁶⁸Ga]Ga-DOTA-FAPI-04 and [¹⁸F] FDG PET/CT for the diagnosis of primary and metastatic lesions in patients with various types of cancer. *Eur J Nucl Med Mol Imaging*. 2020;47:1820–32.
22. Wang L, Tang G, Hu K, et al. Comparison of ⁶⁸Ga-FAPI and ¹⁸F-FDG PET/CT in the evaluation of advanced lung cancer. *Radiology*. 2022;303:191–9.
23. Treglia G, Muoio B, Roustaei H, Kiamanesh Z, Aryana K, Sadeghi R. Head-to-head comparison of fibroblast activation protein inhibitors (FAPi) radiotracers versus [¹⁸F]F-FDG in oncology: a systematic review. *Int J Mol Sci*. 2021;22:11192.
24. Rivera M, Ghossein Ronald A, et al. Histopathologic characterization of radioactive iodine-refractory fluorodeoxyglucose-positron emission tomography-positive thyroid carcinoma. *Cancer*. 2008;113:48–56.
25. Huang R, Pu Y, Huang S, et al. FAPI-PET/CT in cancer imaging: a potential novel molecule of the century. *Front Oncol*. 2022;12:854658.
26. Ballal S, Yadav MP, Roesch F, Raju S, Satapathy S, Sheokand P, Moon ES, Martin M, Agarwal S, Tripathi M, Bal C. 2023. Head-to-head comparison of [⁶⁸Ga]Ga-DOTA.SA.FAPi and [⁶⁸Ga]Ga-DOTANOC PET/CT imaging for the follow-up surveillance of patients with medullary thyroid cancer. *Thyroid*. 2023 May 12. <https://doi.org/10.1089/thy.2023.0008>
27. Ballal S, Yadav MP, Moon ES, et al. Novel fibroblast activation protein inhibitor-based targeted theranostics for radioiodine-refractory differentiated thyroid cancer patients: a pilot study. *Thyroid*. 2022;32:65–77.

Publisher's note Springer Nature remains neutral with regard to jurisdictional claims in published maps and institutional affiliations.

Springer Nature or its licensor (e.g. a society or other partner) holds exclusive rights to this article under a publishing agreement with the author(s) or other rightsholder(s); author self-archiving of the accepted manuscript version of this article is solely governed by the terms of such publishing agreement and applicable law.

Authors and Affiliations

Sanjana Ballal¹ · Madhav P. Yadav¹ · Frank Roesch² · Swayamjeet Satapathy¹ · Euy Sung Moon² · Marcel Martin² · Nicky Wakade¹ · Parvind Sheokand¹ · Madhavi Tripathi¹ · Kunal R. Chandekar¹ · Shipra Agarwal³ · Ranjit Kumar Sahoo⁴ · Sameer Rastogi⁴ · Chandrasekhar Bal¹ 

✉ Chandrasekhar Bal
csbal@hotmail.com

¹ Department of Nuclear Medicine, All India Institute of Medical Sciences, New Delhi, India

² Department of Chemistry, Johannes Gutenberg University, Mainz, Germany

³ Department of Pathology, All India Institute of Medical Sciences, New Delhi, India

⁴ Department of Medical Oncology, BR Ambedkar Rotary Cancer Hospital, All India Institute of Medical Sciences, New Delhi, India